A Non-Reductionist, Homeodynamic Simulator of Ancient-Medicine, Inspired-Artificial Immune Systems for Emergent Intelligence Analysis

Joshika Singh
Independent Researcher
New Delhi, India
ORCID: https://orcid.org/0009-0002-7112-8004

Abstract— **This work presents a mathematically grounded, non-reductionist framework for simulating emergent dynamics in a canonical 10-dimensional ancient medicine-artificial immune inspired system. The system is realized as a stochastic dynamical network with state-dependent drift, adaptive control operators, and hysteresis-based memory, enabling trajectory-level exploration of homeodynamic plasticity. Interventions are modeled as smooth, time-gated operators deforming the state-space geometry without imposing fixed-point constraints. Simulations demonstrate separable pathological regimes, regime-specific stability, and adaptive recovery under structured interventions, illustrating the system's intrinsic self-regulation, non-commutativity, and memory effects. This framework unifies emergent intelligence analysis, trajectory-based disease modeling, and intervention dynamics in a fully differentiable, reproducible computational pipeline, providing a platform for exploring complex adaptive systems beyond traditional reductionist approaches**

Keywords— Homeodynamics, Trajectory-based memory, Emergent intelligence, Hysteresis, Non-commutative control

I. INTRODUCTION

The study of complex adaptive systems often necessitates a non-reductionist approach to capture emergent properties arising from high-dimensional interactions. Inspired by canonical principles of ancient medicine and artificial immune systems (AIS), this work introduces a computational framework that models the dynamics of physiological-like states as a controlled stochastic system. Unlike conventional AIS models, which focus on rule-based or discrete-event dynamics, the proposed simulator encodes plasticity, trajectory-dependent memory, and non-commutative intervention effects within a differentiable, fully continuous state-space. Key system aspects—dimensions—interact via nonlinear couplings and stochastic forcing, producing rich, homeodynamically constrained dynamics. Interventions are implemented as temporally gated, smooth operators, deforming the system's intrinsic trajectories to study adaptive regulation, regime-specific stability, and emergent intelligence. This framework enables quantitative and qualitative analysis of complex systems in a unified, mathematically rigorous manner

II. CONCEPTUAL FRAMEWORK

The proposed simulator has been built upon a set of key principles. These principles define the structural and operational attributes abstracted from the behavior of high-dimensional adaptive dynamical systems.

A. *Intrinsic Dynamical Invariance Principle*

The system is defined on multi-dimensional dynamical control axes which preserve global coherence and stability. These are abstracted from the intrinsic processes of the state space of the system, exhibiting smooth soft regulatory coupling effect rather than rigid deterministic constraint. These invariants act as state-dependent metric modulators that deform and reshape the local geometry across all dimensions upon modulation along any coordinate of state space; resulting in emergent invariance that persists under stochastic perturbations as long as the trajectory of the system remains within the dominant locally contractive regions of the homeodynamic regulatory basin.

B. *Trajectory-Conditioned Non-Hamiltonian Attractor Modulation*

The system behavior is defined by trajectory-dependent dynamics within a thermodynamically open, non-conservative state space, which does not enforce Hamiltonian constraints in order to irreversibly shed accumulated systemic load; thereby preventing pathological load conservation and acting as a functional adaptive mechanism to compel the convergence of the state space towards dynamically viable and stabilized steady states.

The system evolution is shaped by cumulative state history and hysteresis, rather than clock- driven progression; with functional advancement dependent upon the sequence and accumulation of state transformation along with distinct external intervention operators that act as directional biases on trajectories. Their influence is state- configuration dependent with co-evolution which produces coupled feedback as the attractor landscape transforms, thus reshaping gradients. The order and timing of external intervention operators demonstrate non-commutativity. Since progression is trajectory dependent, identical time indices may correspond to different system states despite the parameterization of dynamics using explicit time variables for effective computation.

Various characteristics of the state space vary as a function of internal dimensions and variables, thus resulting in local field warping of the geometry of the space. Rather than discrete failure-condition events, irreversibility arises from basin confinement when system evolution is constrained by the basin geometry of a secondary attractor basin due to reduced probability of trajectory escape upon entry. Thus, degradation is considered as unwanted adaptive drift away from the homeodynamic manifold, characterized by deviation of trajectories from contractive regions and weakening of regulatory coupling, where autonomous recovery becomes dynamically less probable upon entry into an alternative attractor basin instead of the primary homeodynamic attractor. Though within the high coherence region, intrinsic restoring dynamics suffice to guide trajectories into the primary attractor, thus demonstrating the attainment of reversibility and proto-emergent navigation

C. Symmetry-Modulated Predictive Self-Modulation Principle

Along with a perspective, the system is governed by symmetry modulation, specifically soft, state-dependent symmetry modulation, through which local manifold geometry is reconsidered and reconfigured when required. Interventions act as graded symmetry modulators rather than hard corrective forces, enabling adaptive reorganization without enforcing rigid constraints. Through this graded symmetry modulation, alternative dynamical channels are opened that enable controlled escape from maladaptive attractors.

The system operates under a framework of distributed regulation, deploying both short-horizon and long-horizon trajectory processes depending on contextual constraints and regulatory demands. Short-horizon trajectory statistics dominate in locally constrained or rapidly varying regimes, whereas long-horizon trajectory evolution governs slow, structural, and path-dependent processes within the homeodynamic scaffold.

Predictive biases emerge from and are constrained by homeodynamic symmetric scaffolds defined over canonical dimensions, ensuring that anticipatory adjustments remain consistent with system identity and long-term coherence. Internal regulatory fields are adjusted proactively to reduce the stochastic probability of future deviations, thereby enabling effective regulation with minimal intervention effort and reduced thermodynamic dissipation. This mode of self-organization is observable through emergent system-level metrics, including trajectory roughness, hysteresis index, and phase desynchronization.

III. First-Order Canonical Approximation and Assumptions

The dimensions and variables exploited in this framework are not introduced as phenomenological or symbolic labels; they are defined as canonical variables, each corresponding to a distinct regulatory function inherent to a pre-existing canonical organization. These variables act as functional identifiers rather than as constructed, fitted, or learned parameters. Accordingly, the conceptual architecture underlying the present framework is assumed to be prior to and independent of its mathematical reorganization. The simulator presented here constitutes merely a mathematical reorganization and numerical instantiation of this assumed canonical architecture. Therefore, it represents only first order numerical approximation, where the designation first order is neither purely temporal nor perturbative but reflects explicit geometric and algebraic simplifications deliberately adopted to prioritize foundational realization, interpretability, global stability and numerical reproducibility. In its full form, the canonical system admits non-holonomic constraints, intrinsic topological variational dynamics of the trajectory, non-commutative differential logic governing interdimensional coupling, order dependent structural effects, and state-dependent deformation of the admissible domain itself, however, these features are not fully implemented in the current realization.

Instead, stability is enforced as a first order surrogate for intrinsic regulation, and equilibrium is not inferred as an emergent variational extremum of an internal action functional. The simulator operates on a fixed-metric state space with globally bounded trajectories with numerically well-defined solutions. It also employs commutative interaction rules for interdimensional coupling-thereby capturing magnitude dependent interactions while intentionally suppressing order dependent structural effects- and governs state evolution through fixed-form differential relations within a common static admissible domain. Uncertainty is modeled through homogeneous diagonal stochastic perturbations, providing a controlled approximation of variability without inducing stochastic bifurcation or topology-altering fluctuations; this choice linearizes the geometry of uncertainly and excludes state-dependent diffusion effects characteristic of higher order realizations.

IV. The System Architecture And Mathematical Framework

A. Canonical State Space and Dimensions

The system is defined on a finite-dimensional differentiable manifold $\mathcal{M} \subset R^{10}$. The state vector $x(t)$ is composed of ten canonical invariants:

$$x(t) = [A, E, R, D, G, V, P, K, C, Agni]^T. \qquad (1)$$

Where the semantic mapping of the state dimensions and their respective dynamical functions are detailed in Table I. These variables define a primary Homeodynamic Basin $\mathcal{B}0 \subset \mathcal{M}$. Stability is defined as the maintenance of the system trajectory within the primary homeodynamic attractor basin $[x_{min}, x_{max}]$

TABLE I. Canonical State Dimensions And Integrated Mathematical Functions[1]

Dimensions	Mathematical Role
ĀMA(*A*)	Metric stressor: increases local curvature and effective friction; manifold obstruction creating non-contractible regions; symmetry-breaking load introducing irreversibility; topological effect: generates holes/obstructions preventing return to homeodynamic basin
TEJAS(*E*)	Fast gain direction: sharp curvature spikes; manifold destabilizer when unchecked; symmetry-breaking amplifier; topological role: creates Morse-type critical points (activation thresholds)
PRĀṆA (*R*)	Information-flow field: smooths metric entropy; global manifold connector; symmetry-restoring regulator; topological role: reconnects components, prevents fragmentation
DHĀTU (*D*)	Structural density axis: thickens manifold; metric mass term; slow symmetry evolution; topological persistence of cycles and components
KṢETRA (*G*)	Domain variable: defines boundary conditions; manifold embedding; symmetry constraint layer; topological container for all dynamics
VĀTA (*V*)	Transport generator: tangent flow driver; metric destabilizer (oscillation); translation symmetry breaker; topological flow-line generator
PITTA (*P*)	Rate-scaling axis: steepens gradients; manifold time-rescaling; dilation symmetry controller; topological bifurcation timing
KAPHA (*K*)	Metric resistance / inertia: damps curvature and oscillations; manifold cohesion; symmetry-preserving stabilizer; topological robustness of homology
OJAS (*C*)	Attractor depth variable: decreases Lyapunov exponent; manifold resilience; symmetry robustness; topological basin persistence
AGNI(*AGNI*)	Nonlinear gate: induces phase transitions; non-smooth manifold flow; symmetry selection mechanism; topological regime switch

[1] The topological roles described in Table I represent the intended canonical architecture of the framework. In the present first-order numerical realization, these roles are instantiated through state-dependent geometric and dynamical modulations rather than through explicit topological computation; full realization of the underlying topological structure is deferred to higher-order formulations.

B. Non-Hamiltonian Dynamics and The Wrapped Operator

The system evolution is designed to be non-Hamiltonian $(\nabla \times F \neq 0)$ and dissipative. The dynamics are governed by a Wrapped Operator Stochastic Differential Equation (SDE).

1) *The Wrapped Evolution Equation*

The drift field is "wrapped"(bracketed via the projection operator $\Pi_{\mathcal{M}}$ to enforce boundary constraints). The state evolution is given by:

$$dx = \Pi_{\mathcal{M}}\left(F_{int}(x) + \sum_{i=1}^{n} \phi_i(t)\,\mathcal{O}_i(x)\right)dt + \Sigma(x)\,dW_t \quad (2)$$

Where:

F_{int} is the autonomous interaction field.

$\mathcal{O}_i$ are the external intervention operators .

$\phi_i(t)$ are temporal gating functions.

$\Pi_{\mathcal{M}}$ is the Kṣetra Boundary Operator (realized via hard-clipping) ensuring $x \in [0,4.0]^{10}$.

C. Constutive Equations

The autonomous field F_{int} is derived from three specific constitutive relations that bridge the theoretical manifold with the numerical implementation.

1) *The Sigmoidal Gating Function (Soft-Clip)*

The temporal activation gate $\phi(t)$ is introduced to manage regime shifts without numerical discontinuity. Thus, corresponding to the smooth switching logic between different regions of the manifold while avoiding artificial gradient in the simulator:

$$\phi(t; t_s, t_e) = \frac{1}{1 + e^{-k(t-t_s)}} \cdot \frac{1}{1 + e^{k(t-t_e)}} \quad (3)$$

This function ensures differentiability at the edges of intervention windows $[t_s, t_e]$.

k: The slope parameter governing the rate of activation. Larger values of k approximate a hard step function, whereas smaller values yield a smoother, continuously differentiable transition, which improves numerical stability and gradient behavior in JAX-based solvers

2) *Load-Transformation Coupling*

The system's metabolic transformation capacity is modeled as a dynamic state rather than a static parameter. We define the Coupling Coefficient (C_p) to represent the inhibition of Ojas (C) by the cumulative destabilizing load (A). This relationship is governed by a non-linear sigmoid map to ensure the Intrinsic Dynamical Invariants remain bounded under high stress.

$$C_p(x) = \frac{1}{1 + e^{-\lambda(A-C)}} \quad (4)$$

λ :Coupling sensitivity parameter governing sharpness of the transition between load dominated and regulation-dominated regimes. In the underlying ontological mapping, it corresponds to a metabolic threshold of system tolerance; larger values of λ induce a more abrupt suppression of transformation once the threshold is crossed. Specifically, in the implementation:

$$C_p = \sigma\big((V + P + K + \text{Agni}) - (A + E + R + D)\big).$$

The present form of $C_p(x)$ reflects progressive refinement under structural design constraints. Specifically, it must be bounded, smooth, and capable of representing a continuous transition between burden-dominated and regulation-dominated regimes. The sigmoid functional satisfies these requirements while remaining fully differentiable, making it suitable for stochastic dynamical simulation. From an interpretive standpoint, $C_p(x)$ is not treated as an independent state variable but as an emergent functional arising from the interaction of multiple system dimensions. What appears as "capacity" is therefore a relational effect of these interacting processes, rather than an intrinsic property of any single component. In the dynamics, $C_p(x)$ acts as an effective gating variable that modulates downstream behavior according to the instantaneous system balance.

This formulation ensures that when the residual transformational load A significantly exceeds the available systemic potential C, the coupling coefficient C_p asymptotically approaches zero, effectively shunting metabolic transformation to suppress runaway instability.

3) *The Non-Euclidean Metric Deformation*

The state variables representing Vāta (*V*), Pitta (*P*), and Kapha (*K*) define the fundamental coordinate axes of the system's state manifold. A corresponding set of metric modulators is introduced as geometric operators that locally deform the state-space metric by prescribing coordinate-dependent scaling factors for kinetics k_{kin} , transformation k_{trans}, and damping k_{damp} across the *V-P-K* subspace

$$k_{kin}(x) = \mu_V + \gamma_V \cdot \text{clip}(V, 0, V_{max}) \quad (5)$$

$$k_{trans}(x) = \mu_P + \gamma_P \cdot \text{clip}(P, 0, P_{max}) \quad (6)$$

$$k_{damp}(x) = \big(1 + \text{clip}(K, 0, K_{max})\big)^{-1} \quad (7)$$

These scaling factors directly modulate the drift terms of the governing dynamics, selectively influencing the rates of accumulation and systemic clearance. Collectively, they encode a state-dependent geometric reweighting of the system's evolution, conditioned on the underlying Intrinsic Dynamical Invariants.

D. Topological Medicine and Operator Non-Commutativity

Interventions are modeled as state-dependent operators acting on the system dynamics. Each operator induces a local deformation of the underlying metric geometry through the effective scaling relations defined in Eq (5-7). Consequently, intervention operators are non-commutative, reflecting the critical order-sensitivity of systemic modulation.

$$[\mathcal{O}_1, \mathcal{O}_2] = \mathcal{O}_1 \circ \mathcal{O}_2 - \mathcal{O}_2 \circ \mathcal{O}_1 \neq 0 \quad (8)$$

E. Formal Definitions of Systemic Intelligence

Definition 1 (Emergent Intelligence):

A system exhibits emergent intelligence if it possesses an internal mechanism for Autonomous Flow Deformation. When a perturbation δx displaces the state outside the nominal homeodynamic basin $\mathcal{B}_0$, the system generates a corrective field $\widetilde{\Phi}_t$ that re-enters the stable region without external optimization.

$$x(0) + \delta x \notin \mathcal{B}_0 \Rightarrow \widetilde{\Phi_t}(x(0) + \delta x) \in \mathcal{B}_0,\ t > 0 \tag{9}$$

Definition 2 (Constructive Learning):

Constructive learning is defined as a topological deformation of the system's regulatory geometry in which the system's regulatory capacity increases. This is quantified by the growth of the basin volume $\mathcal{V}$.

$$\Delta\mathcal{V}(\mathcal{B}_\Gamma) = \mathcal{V}(\mathcal{B}_\Gamma) - \mathcal{V}(\mathcal{B}_0) > 0 \tag{10}$$

Hysteresis is defined as the non-vanishing path-dependency of the state manifold. It signifies that the system's response to an intervention is not a simple reversible function of the current input, but is instead integrated over the history of the Metric Modulators. This path-dependency is what allows for the emergence of "Constructive Learning," where the volume of the viable homeodynamic basin $\mathcal{B}_0$ expands following a closed intervention cycle Γ

The hysteresis functional $\mathcal{H}$ captures the "work" done by the intervention operators on the system manifold. For a system to exhibit memory and learning, the integration of the state deformation across a closed loop must be non-zero.

The Hysteresis Function

$$\mathcal{H} = \oint_\Gamma x \cdot dF \neq 0 \tag{11}$$

$\mathcal{H}$: The Hysteresis Functional, representing the total structural shift or "learned" information captured by the system.

The Contour Integral over a closed intervention trajectory Γ, indicating that the calculation accounts for the entire sequence of state transformations.

x: The State Vector, defined by the coordinates of Vata (*V*), Pitta (*P*), and Kapha (*K*).

dF: The Differential Forcing Vector, representing the influence of the non-commutative intervention operators $\mathcal{O}$ on the manifold.

V. COMPUTATIONAL REALISATION

The simulator is realized as a controlled stochastic dynamical system numerically integrated using the Diffrax framework within the JAX ecosystem. The system is formulated as a stochastic differential equation (SDE) comprising a deterministic drift field and additive diagonal diffusion.

1. *Numerical Integration and Stability*

A Heun integrator is employed for time integration, providing strong-order convergence (0.5). Unlike weak-order solvers that only capture distributional moments, this strong-order consistency is essential for the path-wise analysis of Intrinsic Dynamical Invariants at the individual trajectory level. Adaptive step-size control is enforced via a proportional–integral–derivative (PID) controller. This prevents the numerical "step-size hunting" common in standard adaptive schemes, ensuring smooth temporal resolution transitions in regions of locally induced stiffness arising from state-dependent coefficient modulation.

2. Stochastic Consistency and Reproducibility

Stochastic forcing is implemented using a Virtual Brownian Tree (VBT), which provides O(1) memory overhead relative to time. The VBT ensures seed-invariant stochastic trajectories across varying solver step sizes; the Brownian path at any query time t remains fixed and independent of internal solver discretization. This construction guarantees temporal consistency of noise realization, permitting reproducible comparisons of intervention strategies (Krama) under identical "unfolding" of stochastic conditions. Output sampling is decoupled from internal adaptive steps through fixed observation grids, preventing sampling bias that might otherwise occur due to step clustering in high-volatility regimes.

3. Control Operators and Non-Commutativity

Intervention operators are incorporated as smooth, sigmoid-gated control inputs acting directly on the drift field. This design replaces discrete switching logic with C^∞ differentiable envelopes, preserving solver stability and allowing the JAX XLA compiler to perform kernel fusion for maximum computational throughput. Overlapping intervention windows compose additively into a single composite vector field. This yields non-commutative sequencing effects at the trajectory level: because the state y at t_2 is a function of the intervention applied at t_1, the path-integral is sensitive to operator ordering.

4. Geometry and Manifold Constraints

State-space geometry is dynamically modulated through state-dependent kinetic, transport, and damping coefficients, inducing a local metric warping. Computationally, this induces a non-Euclidean landscape where the adaptive solver acts as a dynamic re-gridding mechanism to maintain accuracy across variable curvature. Linear projection operators regulate coupled subspaces (e.g., Dosha balance) by projecting the state onto a constrained manifold. This null-space projection prevents drift away from physiological regimes without introducing discrete conditional branching, effectively reducing the system's rank and enhancing numerical stability.

5. Bounds and Differentiability

Explicit state clipping is applied solely as a numerical safety bound to prevent non-physical excursions and is not treated as a dynamical operator; it introduces zero-gradient zones at the boundaries (y=0, 4) which are accounted for during sensitivity analysis. The use of a diagonal linear operator for diffusion enforces independent noise across dimensions, reducing the complexity of the stochastic calculus from O(N^2) to O(N) and focusing the computational load on the coupled deterministic drift.

All components are expressed using JAX-compatible primitives, rendering the entire numerical pipeline fully differentiable. This enables the computation of exact gradients (e.g., ∂Recovery/ ∂Dosha_Shift) for sensitivity analysis and optimization. No post-processing or smoothing is applied to the outputs, ensuring that the reported trajectories reflect the raw, intrinsic dynamics of the system.

Interpretive note: The present model should be interpreted as a first-order geometric realization of a topology- inspired invariance principle, where structural persistence is encoded through state-dependent dynamics rather than explicit topological computation.

VI. EXPERIMENTS AND RESULTS

A. Experimental Objectives

The experiments aim to demonstrate qualitative and quantitative system-level properties of the proposed simulator, rather than to optimize or clinically validate therapies. Specifically, the experiments examine state-space separability, internal homeodynamic regulation, adaptive immune-like plasticity, hysteresis-based memory, and interpretation of disease as a dynamical regime with intervention acting as controlled geometric deformation.

TABLE II. BASELINE REGIME METRICS

Epilepsy Type	Mean Step Size	Step Variability	Top Eigenvalue	Variance Growth Rate	Hysteresis Index	Phase coherence	Roughness Index
Vātaja	0.017	0.01082	0.31892	0.000245	0.8357	0.71078	0.75491
Pittaja	0.0151	0.00679	0.14396	0.000249	0.61918	0.75117	0.669
Kaphaja	0.01411	0.00596	0.20079	0.000286	0.74738	0.73648	0.62601
Sannipātaja	0.01646	0.01269	0.32633	0.000317	0.80339	0.69969	0.80251

B. Regime Selection

Epilepsy (Apasmara) was selected as a representative nonlinear, episodic, and system-level disorder. Four regimes were instantiated via normalized, dimensionless initial conditions: Vātaja, Pittaja, Kaphaja, and Sannipātaja epilepsy, corresponding to distinct regions of the simulator's state space.

C. Experiment I: Baseline Dynamics (No Intervention)

This experiment evaluates whether structured initial-condition biases alone are sufficient to generate distinct and reproducible dynamical regimes under identical stochastic forcing and zero external intervention. The objective is to verify that regime differentiation arises intrinsically from the system's coupling structure rather than from parameter tuning or external control.

The baseline reference state:

$$y_0 = [0.1, 0.1, 1.0, 0.0, 1.0, 1.0, 0.33, 0.33, 0.34, 1.0]^T$$

instantiates a dynamically stabilized configuration of the system. Regulation is maintained through the interaction between E and, R where the negative feedback term proportional to $0.1 \cdot \frac{R}{E+0.1} \cdot E$ moderates effector growth and prevents instability. The nonlinear gate $Agni$ ensures that transformation and clearance mechanisms remain active, allowing efficient dissipation of A through the term. $trans \cdot Agni \cdot E \cdot A$ .The geometric modulators (V, P, K) are initialized in a near-symmetric configuration, producing balanced kinetic scaling, transformation rate, and damping through the state-dependent warping function. The domain variables remain aligned with the reference manifold via clearance dynamics, ensuring bounded evolution around the intrinsic target state. Collectively, this configuration represents a regime in which growth, dissipation, and regulation remain in equilibrium.

Four regime hypotheses are instantiated as directional perturbations from this reference:

$$y_{\text{Vātaja}} = [0.75, 0.1, 0.75, 0.1, 1.0, 1.0, 1.08, 0.43, 0.29, 0.85]^T.$$

$$y_{\text{Pittaja}} = [0.13, 0.1, 0.98, 0.03, 1.0, 1.0, 0.35, 0.37, 0.34, 0.99]^T$$

$$y_{\text{Kaphaja}} = [0.29, 0.1, 0.74, 0.32, 1.0, 1.0, 0.33, 0.46, 1.11, 0.55]^T$$

$$y_{\text{Sannipātaja}} = [0.91, 0.1, 0.37, 0.63, 1.0, 1.0, 0.87, 0.78, 1.20, 0.64]^T$$

A damping K weakens stabilization, producing amplification-dominated dynamics. In the Pittaja regime, near-baseline influence of A with preserved R and effective $Agni$ mediated transformation, maintains strong transformation and regulation, resulting in smoother trajectories. In the Kaphaja regime, the system dynamics are predominantly governed by the damping influence of K, while reduced $Agni$ mediated transformation weakens the clearance term $trans \cdot Agni \cdot E \cdot A$, resulting in increased persistence and reduced variability. In the Sannipātaja regime, simultaneous strengthening of the influence of A,D, and all geometric modulators (V,P,K) reduces coupling coherence across growth, transformation, and damping processes, producing highly irregular dynamics.

These initializations are not obtained through optimization or data fitting; they represent hypothesis-driven perturbations of the system's internal geometry.Trajectory-based metrics—including roughness, hysteresis index, phase coherence, and variance growth—are computed from the stochastic evolution following initialization. As shown in Fig. 1 and Table II, regimes with amplified growth and reduced damping exhibit higher roughness and variability, while damping-dominated regimes display smoother but more persistent trajectories with increased hysteresis. These results confirm that state-space separability and regime-specific dynamics emerge intrinsically from the system's non-linear coupling structure rather than from externally imposed objectives or parameter tuning.

D. Experiment II: Structured Intervention

A staged Deepana–Shamana intervention was applied to the Vātaja initial configuration at severity 1.5. Deepana was active from t=15 to t=25 and Shamana from t=20 to t=40, with overlapping windows creating a composite operator field consistent with the non-commutative formulation in Equation 8. Phase-wise mean state values were extracted across four temporal windows: pre-intervention, Deepana-active, combined Deepana-Shamana, and post-intervention.

Āma reduction proceeded similarly with and without intervention-from 0.502 pre-intervention to approximately-0.291 post-intervention in both runs-demonstrating that intrinsic regulatory dynamics govern accumulated metric stressor clearance autonomously, consistent with the emergent intelligence defined in Definition 1. The substantive effect of the intervention appeared in the Dosha subspace (V-P-K subspace): without medicine, post-intervention Vāta, Pitta, Kapha stabilized at 1.116, 1.086, and 1.066, respectively, remaining substantially elevated above their baseline configuration at simulation initialization. Under the staged intervention, these values shifted to 1.330, 0.716, and 1.223, indicating a measurable deformation of the terminal trajectory within the V-P-K subspace, consistent with the state-dependent metric modulation described in Equations 5-7.

Recovery emerged through continuous trajectory deformation rather than convergence to a fixed point, preserving dynamical variability while restoring bounded evolution within the homeodynamic basin. This behavior is illustrated in Fig.1

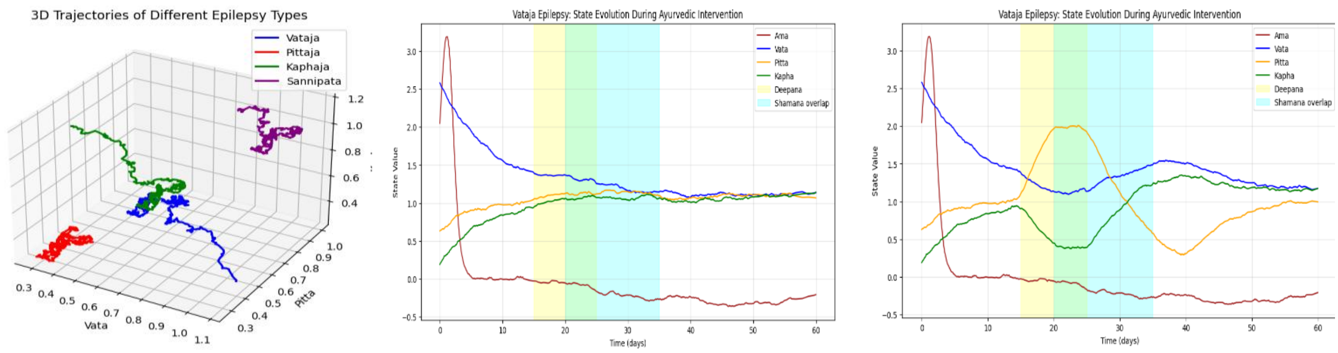

Fig.1-(a) 3D trajectories of different dynamical archetypes in the canonical ontological state-space (Vata–Pitta–Kapha axes). Each colored line represents the progression of the internal dynamical state for one type of archetype: Vataja (blue), Pittaja (red), Kaphaja (green), and Sannipata (purple). Start and end points are indicated implicitly by the line direction. This visualization highlights the separability among the archetypes in the multidimensional state space and allows qualitative comparison of trajectory spread, curvature, and overlap across regimes, consistent with Table II. (b) Temporal evolution of key physiologically-inspired states (Āma, Vāta, Pitta, Kapha) in a Vataja epilepsy like regime under no intervention. (c) Under Deepana-Shamana intervention. Shaded regions indicate intervention periods: yellow for Deepana, cyan for overlapping Shamana. The graph illustrates the system's response and adaptive regulation during treatment.

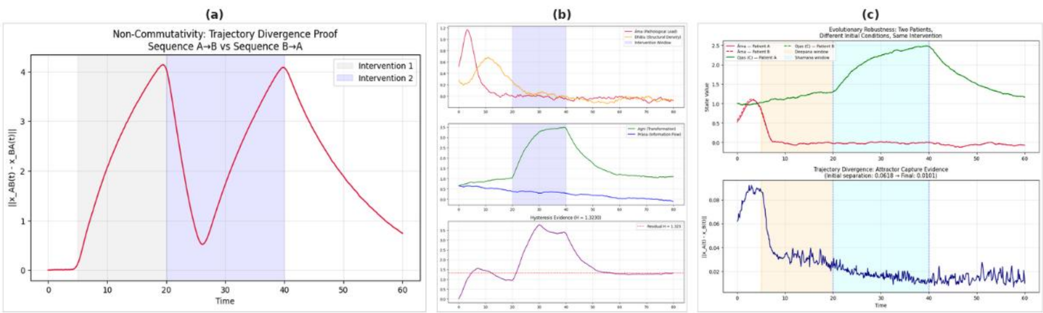

Fig.2.Three complementary tests of memory-bearing dynamics in the proposed framework. (a) Non-commutativity: reversing the intervention order produces persistent trajectory divergence under identical stochastic forcing, and solver settings. (b) Hysteresis proxy: a closed intervention cycle leaves a non-zero residual deviation from the initial state, indicating structural memory in the first-order realization. (c) Evolutionary robustness: two nearby initial configurations converge toward a common bounded region under the same staged intervention, demonstrating attractor capture and plastic stability. Together, the panels provide operational evidence of path dependence, residual memory, and bounded robustness in a non-Hamiltonian, trajectory-conditioned dynamical system.

E. Experiment III: Path Dependence, Non-Commutativity, and Evolutionary Robustness

1.Objective

Experiment III investigates three interdependent properties of the proposed dynamical framework; evolutionary robustness through attractor capture, hysteresis as structural memory, and operator non-commutativity as trajectory-conditioned path dependence. Together, they provide operational evidence consistent with Definitions 1 and 2 and Equation 11 of the formal framework.

2. Setup

All sub-experiments share the same Vātaja initial state base vector:

$$x_0 = [0.1,0.1,1.0,0.0,1.0,1.0,0.33,0.33,0.34,1.0]^T$$

With a perturbation of scale 0.7 applied across the ĀMA, PRĀṆA, DHĀTU, VĀTA, PITTA, KAPHA and AGNI dimensions, clipped to the admissible domain $[0,4]^{10}$. A fixed random seed ensures stochastic reproducibility across all parts. The Vātaja regime was selected as a representative case study for this experiment. The simulator code provided in the accompanying repository may be adapted to explore additional regimes.

3.Part A-Evolutionary Robustness and Attractor Capture

Two simulation trajectories, denoted A and B for notational clarity, are initialized from the Vātaja state with an additional perturbation applied to B, yielding an initial separation of $x_A(0) - x_B(0) = 0.0618$. Both receive an identical staged Deepana-Shamana intervention under identical stochastic forcing. Trajectory divergence is computed as $|x_A(t) - x_B(t)|$ across the simulation window.

The divergence rises briefly to a peak of 0.0920 during the Deepana window before decreasing monotonically to a final value of 0.0101, giving a convergence ratio of 0.1634. This means the terminal separation between the two trajectories is only 16.3% of the initial separation, indicating that the shared intervention guides both trajectories into the same contractive homeodynamic region without enforcing fixed-point convergence. This provides evidence of attractor capture and functional robustness under varied Vātaja initial configuration.

4. Part B-Hysteresis and Structural Memory

A closed intervention cycle is applied in three phases: no intervention (t=0-20), Deepana-Shamana (t=20-40), and unforced recovery (t=40-80). A memory-free system would be expected to return to its initial state after removal of external forcing. Instead, the terminal state norm (1.8374) differs measurably from the initial norm (2.0068). The residual state deviation yields a proxy hysteresis value $\mathcal{H} = 1.3230 \neq 0$.

The formal contour integral in Equation 11 is retained as the theoretical reference for the higher-order canonical architecture; in the present first-order realization, residual state deviation serves as the operational proxy. The distance from the initial state stabilizes persistently above zero in the post-intervention phase, indicating a residual shift in the regulatory geometry and supporting the interpretation of structural memory.

5. Part C-Operator Non-Commutativity

Two simulations start from identical conditions with identical stochastic forcing. Simulation AB applies Deepana from t=5 to t=20 followed by Shamana from t=20 to t=40; Simulation BA applies the same interventions in reverse order. The trajectory $|x_{AB}(t) - x_{BA}(t)|$ is computed across the full simulation window.

The divergence begins at zero, confirming identical initialization. It rises to a first peak of approximately 4.1 near t=20, partially recovers around t=26, rises again to approximately 4.1 near t=40, and finally stabilizes at 0.7405 rather than returning to zero. The maximum observed divergence is 4.135. This persistent non-zero residual indicates that the two intervention sequences produce irreducibly different terminal states despite identical total intervention content, consistent with non-commutative operator behavior.

6. Interpretation

The three parts collectively indicate that robustness and path dependence coexist within the proposed framework. Part A establishes plastic stability: varied initial configurations converge under shared intervention. Part B indicates a persistent residual shift after a closed intervention cycle, consistent with structural memory. Part C demonstrates order-sensitive divergence: identical total intervention content produces measurably different outcomes when applied in different sequences. The underlying geometric structure is inferred operationally through trajectory divergence and residual state deviation, consistent with the first-order realization described in Section III, and is conceptually analogous to inferring curvature from geodesic deviation, though the analogy is heuristic rather than formal. Taken together, these results support the interpretation of the simulator as a memory-bearing, path-dependent adaptive system exhibiting emergent intelligence as defined in Section IV.E. Results are shown in Fig2.

VII. Discussion and Conclusion

This work presents an architectural rather than algorithmic contribution to the study of complex adaptive systems. Instead of encoding behavior through optimization objectives, learning rules, or explicit decision logic, the framework enables robustness, structural memory, and emergent intelligence to arise intrinsically from a coupled stochastic dynamical system evolving on a non-Hamiltonian manifold. This non-reductionist formulation, where coherence emerges from geometric state-dependent interactions, aligns with established perspectives in complex systems research. The proposed framework is not a data-driven physiological model but an architectural abstraction derived from ontological mapping; the variables represent equivalence classes of dynamical behavior rather than directly measurable biological quantities, and no clinical interpretation is implied. Consequently, validation is achieved through the verification of emergent dynamical properties-such as non-commutativity and structural memory-rather than through curve-fitting to empirical datasets.

The approach addresses a structural limitation in conventional artificial immune systems and pharmacokinetic models, which treat operator effects as additive and order-independent. Such models typically preclude the representation of path-dependent intervention sequences. In this framework, interventions are constructed as non-commutative geometric transformations, such that $[\mathcal{O}_1, \mathcal{O}_2] \neq 0$, emerging directly from the trajectory-conditioned dynamics. Experiment III confirms this with a maximum divergence of 4.135 and a terminal separation of 0.7405 under reversed operator sequences. Evolutionary robustness is further supported through attractor capture, with a convergence ratio of 0.1634 between distinct initial states under shared intervention.

Memory is encoded as path-dependency of the state manifold rather than an explicit stored variable. System response integrates over prior metric modulation, producing a non-zero hysteresis functional after a closed intervention cycle ($\mathcal{H} = 1.3230$). Memory is thus structural, arising from geometric deformation rather than a retrieval mechanism, which is consistent with the formal definition of Constructive Learning.

The dimensional structure is organized via an ontological mapping to a structured hierarchical framework, used as an interpretive scaffold without implying direct physiological correspondence. Pathological states are therefore modeled as dynamical regimes characterized by weakened coupling and reduced basin contractivity. Crucially, the homeodynamic basin is interpreted as an emergent region of intrinsic trajectory convergence sustained by the state-space geometry itself, independent of external objectives. Interventions act as geometric operators that reshape these trajectory manifolds without enforcing fixed-point convergence.

A 10-dimensional Ayurvedic AIS simulator based on this formulation reproduces regime-specific dynamics, homeodynamic plasticity, operator non-commutativity, and structural memory effects. This establishes a reproducible, non-reductionist computational methodology for analyzing adaptive, memory-bearing dynamics in high-dimensional stochastic systems. Future work will extend this framework to multi-regime interventions, parameter sensitivity studies, and data-driven calibration.

VIII. CODE AVAILIBILTY

The simulator is implemented in Python using JAX and Diffrax. The complete source code and reproducible Google Colab notebooks are publicly available via the GitHub repository, with a citable archived version provided through Zenodo:

GitHub-repository: https://github.com/singh-research/research-notebooks

Zenodo DOI: https://doi.org/10.5281/zenodo.19587658

The Zenodo archive corresponds to the version used in this study and ensures long-term reproducibility of the reported results.

REFERENCES

[1] de Castro, L.N., & Von Zuben, F.J. (2002). Artificial Immune Systems: Part I – Basic Theory and Applications. BioSystems, 64(1–3), 1–19.

[2] Dasgupta, D. (Ed.). (1999). Artificial Immune Systems and Their Applications. Springer.

[3] Y. Song, J. Yuan, and X. Pang, "SAIS: A Novel Bio-Inspired Artificial Immune System Based on Symbiotic Paradigm," in Companion Conf. on Genetic and Evolutionary Computation (GECCO '24), 2024, pp. 240–243. doi: 10.1145/3638530.3664188

[4] L. Kong, J. R. Brewer, and Y. C. Lai, "Reservoir-computing based associative memory and itinerancy for complex dynamical attractors," Nat. Commun., vol. 15, no. 1, p. 4840, 2024. doi: 10.1038/s41467-024-49190-4.

[5] Kauffman, S.A. (1993). The Origins of Order: Self-Organization and Selection in Evolution. Oxford University Press.

[6] Farmer, J.D., Packard, N.H., & Perelson, A.S. (1986). The immune system, adaptation, and machine learning. Physica D, 22, 187–204.

[7] S. Balachandran, M. Holmberg, and N. Lakemond, "Understanding the development of emerging complex intelligent systems," J. Eng. Technol. Manage., vol. 72, p. 101815, 2024. doi: 10.1016/j.jengtecman.2024.101815